Journal of Nuclear Materials 402 (2010) 87–92

Contents lists available at ScienceDirect

Journal of Nuclear Materials

journal homepage: www.elsevier.com/locate/jnucmat

He implantation in cubic zirconia: Deleterious effect of thermal annealing

G. Velisa [a,*], A. Debelle [b], L. Vincent [b], L. Thomé [b], A. Declémy [c], D. Pantelica [a]

[a] National Institute for Physics and Nuclear Engineering – "Horia Hulubei", 407 Atomistilor St., Magurele-Ilfov, P.O. Box MG-6, 077125, Romania
[b] Centre de Spectrométrie Nucléaire et de Spectrométrie de Masse, UMR8609, Bât. 108, 91405 Orsay, France
[c] Laboratoire de Physique des Matériaux, UMR6630, CNRS-Université de Poitiers, BP 30179, F-86962 Futuroscope-Chasseneuil Cedex, France

ARTICLE INFO

Article history:
Received 29 January 2010
Accepted 2 May 2010

ABSTRACT

This study investigates the microstructural modifications induced in cubic zirconia by He implantation at high concentration (~4 at.%). The effect of post-implantation thermal annealing on the crystal stability is particularly addressed. For this purpose, three complementary analysis techniques, namely RBS/C, XRD and TEM, have been used. The structure of as-implanted crystals appears weakly defective, the damage very likely consisting of interstitial-type defects and helium-vacancy clusters. These defects induce a tensile elastic strain gradient with a depth distribution that overlaps the He depth profile. After annealing at 800 °C, a partial strain relaxation is observed, but the crystalline structure is strongly altered due to the formation of helium bubbles and elongated fractures.

1. Introduction

Zirconia stabilized in the cubic phase is considered as a potential inert matrix for actinide immobilization. In the framework of this recent concept of long-term storage of nuclear waste, the effect of self-irradiation by the alpha decay of actinides incorporated in the immobilization matrices is a problem that needs to be tackled. Indeed, this phenomenon leads to the production of both low-energy heavy nuclei (alpha recoils) and high-energy alpha particles. The alpha recoils are responsible for most of the crystal damage through elastic nuclear collisions, but the strong resistance of cubic zirconia against low-energy heavy-ion irradiation, simulating recoil nuclei, has been extensively demonstrated [1–6]. On the contrary, alpha particles have weak direct irradiation impact. Nevertheless, their concentration can reach more than 1 at.% over a long storage period, and the presence of a large helium concentration in crystalline matrices usually leads to detrimental microstructural modifications inducing deleterious effects on the matrix mechanical properties ([7] and references therein). Yet, the behavior of He in cubic zirconia has retained less attention and only very few studies dealt with this topic [6,8–15].

It has been demonstrated that, similarly to what happens in metals, helium implanted in yttria-stabilized (cubic) zirconia (YSZ) is trapped at irradiation-induced vacancy-like defects [8–11] or even at native oxygen vacancies [11]. Furthermore, the damage build-up has been established [6,12]. A two-step behavior was found: at low He concentration (typically below ~1 at.%) where the radiation damage consists of isolated defect clusters; at higher He concentration, the damage is mostly related to the formation of nanometre-sized gas bubbles. Due to these initial different microstructures, the helium behavior upon annealing was also found to be helium concentration dependent [9–11]. Actually, in the low-concentration range, it seems that the helium-vacancy clusters dissociate and a helium release is measured at a temperature as low as ~400 °C [9,12]. Conversely, in the high-concentration range, the formation of helium bubbles is always invoked, although very few studies presented micrographs of He bubbles (see e.g. [13,14] where He bubbles are observed in polycrystalline $MgAl_2O_4$–YSZ composite materials). The Ostwald ripening mechanism was proposed to account for the bubble growth [9]. The surface morphology modifications of implanted and annealed crystals were also investigated, and the formation of blisters due to the presence of helium bubbles was clearly shown [15]. These authors also put forward the importance of the helium concentration on the morphology and amount of surface damage.

The current paper presents a study of the damage induced in He-implanted YSZ single crystals in the regime where the destabilization of the crystal is mostly related to the presence of a large He concentration in the YSZ lattice. According to previous work [6,13], the corresponding He concentration must be larger than ~1–2 at.%. The microstructural modifications induced by He implantation in both as-implanted and annealed YSZ single crystals are characterized, and their effect on the matrix integrity are examined. For this purpose, three complementary analysis techniques were used: (i) Rutherford Backscattering Spectrometry and Channeling (RBS/C) associated with Monte–Carlo simulations to determine the damage depth profiles, (ii) X-ray Diffraction (XRD) to measure the elastic strain, and (iii) Transmission Electron Microscopy (TEM) to observe the microstructural modifications, e.g. the formation of bubbles.

* Corresponding author. Tel.: +40 21 404 23 32; fax: +40 21 457 41 11.
E-mail address: gihan@tandem.nipne.ro (G. Velisa).

0022-3115/$ - see front matter © 2010 Elsevier B.V. All rights reserved.
doi:10.1016/j.jnucmat.2010.05.001

2. Experimental

The samples used in this study are (1 0 0)-oriented cubic zirconia single crystals fully stabilized with 9.5 mol% yttria, synthesized by the Crystal GmbH company in Berlin. Crystals were implanted at room temperature (RT) with 30 keV He ions to a fluence of 5×10^{16} cm^{-2} in a random direction (by tilting the crystals with an angle of 7° relatively to the surface normal). SRIM calculations [16] indicate a maximum atomic He concentration of ~4 at.% at a depth of ~160 nm, and a maximum damage dose of ~1.7 displacement per atom (dpa) at ~150 nm. After implantation, crystals were thermally annealed under vacuum for 1 h at 800 °C in a standard tubular furnace.

Prior to RBS/C analysis, the samples were covered with a ~15 nm thick carbon layer to avoid charging effects. The RBS/C experiments were performed by using a $^4He^+$ beam at an energy of 1.6 MeV. The energy resolution of the experimental setup was about 15 keV. The depth distribution of the accumulated damage (f_D) was extracted from the analysis of RBS/C spectra with Monte–Carlo simulations performed by using the McChasy computer code [17]. Implantations and RBS/C experiments were performed with the JANNuS facility of the CSNSM in Orsay.

XRD measurements (θ–2θ scans) were carried out in the Bragg reflection geometry on an automated laboratory-made two circle goniometer (PhyMat – Poitiers). This device is equipped with a sample holder with two rotation axes stages allowing to precisely align the single crystals. A 5 kW RIGAKU RU-200 generator provides Cu radiations, and a quartz plate allows the selection of the Cu Kα1 ray (λ = 0.15405 nm).

Cross-sectional TEM (XTEM) samples were prepared by mechanical polishing using the tripod technique [18]. Finally, a ~7 nm thick carbon layer was deposited on the surface of all samples to prevent charging effects during TEM experiments. Conventional TEM observations were carried out with a Tecnai G220 microscope operating at 200 keV.

3. Results

3.1. Microstructure of as-implanted crystals

RBS/C spectra recorded on YSZ crystals before and after implantation with 30 keV He ions at a fluence of 5×10^{16} cm^{-2} are represented in Fig. 1a. Two plateaus (below 1400 and 600 keV), which correspond to the backscattering of He particles from, respectively, the Zr and O atoms of YSZ, are exhibited on the spectrum registered in a (rotating) random direction (filled circles). The channeling effect is evidenced by the much lower backscattering yield in both the Zr and O sublattices obtained for the spectrum taken on a virgin YSZ crystal with the He beam aligned along the ⟨1 0 0⟩ axis (open circles). An increase of both the Zr and O yields, due to the creation of radiation damage, is exhibited on the ⟨1 0 0⟩-aligned spectrum recorded on the implanted sample (open triangles). The presence of a "damage peak" is particularly visible in the Zr sublattice (at an energy of 1210 keV). RBS/C data may be fitted (solid lines in Fig. 1a) by using the McChasy Monte–Carlo simulation code in order to extract disorder depth profiles [17]. Calculations rely on the basic assumption that a fraction of (Zr and O) atoms are randomly displaced from their original lattice site during ion implantation. A very good agreement is observed between fits and experimental spectra. Depth distributions of the damage accumulated in the Zr sublattice of YSZ crystals (f_D), as extracted from McChasy simulations, are presented in Fig. 1b. The maximum of the damage peak is located around 130 nm, i.e. very close to the maximum of the SRIM-predicted dpa peak (~150 nm). It is worth emphasizing that the disorder level is weak at this maximum ($f_D \sim 0.3$). Similar results (not shown here) have been obtained for the O sublattice.

θ–2θ experimental scans recorded in the vicinity of the (4 0 0) Bragg reflection are displayed in Fig. 2a for virgin and implanted zirconia crystals. The (logarithmic) intensity distributions are also plotted as a function of ε_N, the elastic strain in the direction normal to the surface of the samples. At $\varepsilon_N = 0$ ($2\theta \sim 73.6°$), a sharp and intense diffraction peak coming from the diffraction by the unperturbed bulk YSZ crystal is recorded. This peak is taken as an internal strain gauge to quantify the normal strain. The implanted zirconia layer gives rise to a scattered intensity visible at lower 2θ angles ($\varepsilon_N > 0$ values). This result indicates that the implanted layer is characterized by a larger lattice parameter than the bulk one. In other words, a tensile strain is created along the normal to the crystal surface. This result is in agreement with previous investigations in YSZ irradiated under different conditions [19,20]. Moreover, the scattered intensity exhibits a fringe pattern, revealing the presence of a strain depth distribution. Since the fringe spacing is directly related to the width of the strained region ($\Delta z = 1/\Delta K$, where K is the magnitude of the scattering vector, $2\sin\theta/\lambda$), the depth strain distribution can be reconstructed [21]. In the present case, it is found that the shape of the strain depth profile is very similar to the SRIM-predicted He depth distribution (see Fig. 2b). This feature has also been observed in low-energy He-implanted 6H-SiC single crystals [22]. It is worth mentioning that the θ–2θ scans do not provide any information about the absolute depth scale of the strain profile, but, due to the strong similarity between the SRIM-predicted He profile and the strain profile, this latter profile has been located at the same depth as the former. This strain depth distribution is characterized by a Gaussian-like shape with a FWHM of ~130 nm. The maximum strain level reaches 1.6%. This value is low as compared to that measured in e.g. SiC [22]), but is typical for YSZ, as already observed under other different irradiation conditions: 0.55% for 4 MeV Au [19] and 1.2% for 300 keV Cs [20]. Rocking-curves (ω-scans) recorded on the virgin crystal and on the strained ($\varepsilon_N \sim 0.2\%$), thus damaged, part of the implanted sample are presented in the inset of Fig. 2a. Implantation induces only a slight broadening of the peak with respect to that recorded for the virgin crystal. This result indicates that the implanted layer is still crystalline, as it was already demonstrated by RBS/C. Furthermore, this weak diffuse scattering strongly suggests the presence of radiation defects with a small dimension.

The microstructural damage evidenced by both RBS/C and XRD on as-implanted YSZ samples was observed by XTEM (see Fig. 3a). On this figure, the variation of the contrast as a function of the depth indicates that the crystal is slightly damaged from the surface up to ~100 nm, and that the main defective zone is centered at a depth of ~140 nm, in good agreement with the location of the maximum of both f_D (~130 nm, see Fig. 1b) and dpa (~150 nm) parameters. This micrograph also confirms the absence of amorphization, as already suggested by RBS/C and XRD measurements. The contrast shows strain fields in the defective part of the crystal arising from the presence of point defect clusters; this observation is consistent with XRD (ω-scans) measurements. Over and under-focused images did not reveal the presence of He bubbles (He-vacancy clusters with a size smaller than ~1 nm cannot be detected).

3.2. Microstructure of annealed crystals

Fig. 1a shows a RBS/C spectrum recorded on a YSZ crystal implanted with He ions at RT and subsequently annealed at 800 °C. A surprising but significant increase of the channeling yield is observed for the Zr and O sublattices, as compared to that obtained for the as-implanted sample. Both the surface region and the region where He is implanted appear to be more damaged than before annealing. This effect is confirmed by Fig. 1b which presents

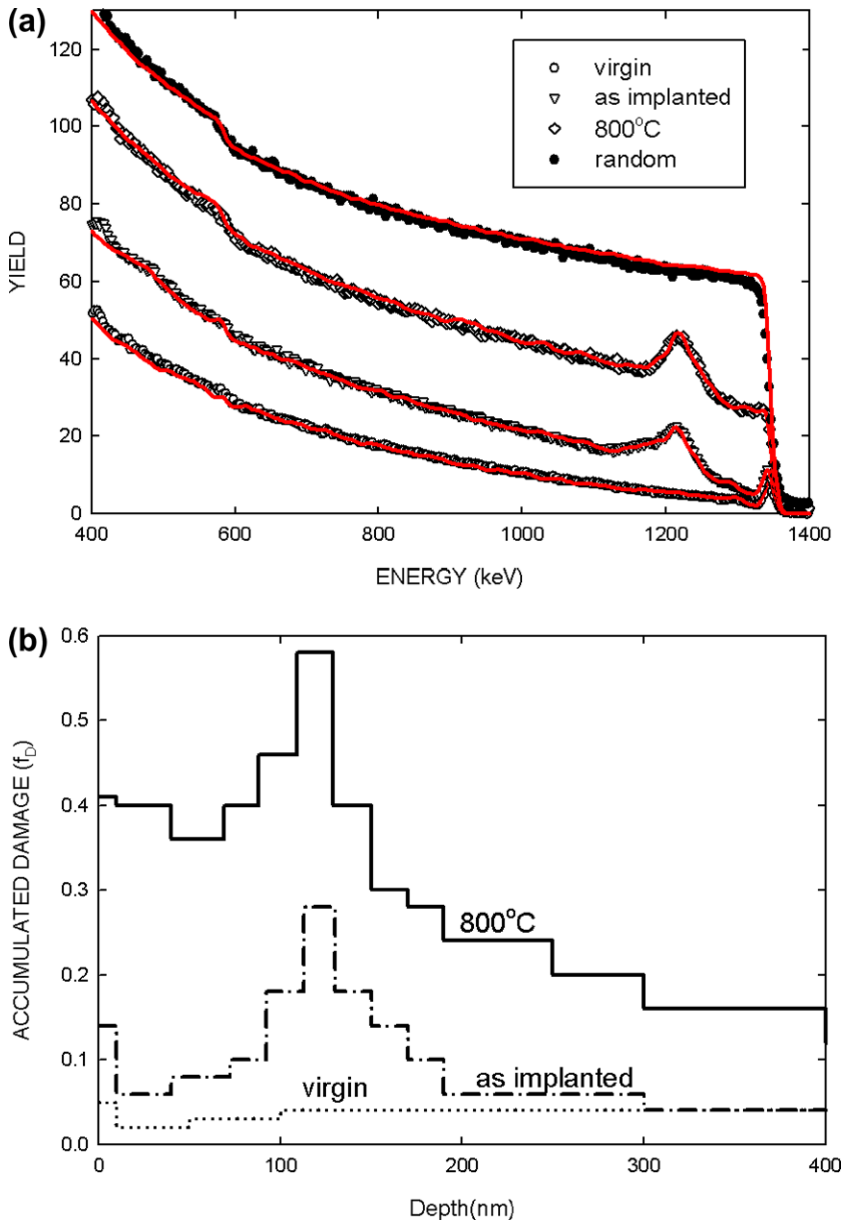

Fig. 1. (a) RBS spectra recorded in random (filled symbols) and ⟨1 0 0⟩ axial (open symbols) directions on YSZ single crystals implanted at RT with 30 keV He ions at 5×10^{16} cm^{-2} and annealed for 1 h at 800 °C. Solid lines are fits to RBS spectra with McChasy simulations. Energy of the analyzing ^{4}He beam: 1.6 MeV. (b) Damage depth profiles in the Zr sublattice of YSZ extracted from the analysis of RBS spectra of Fig. 1a.

the depth distribution of the accumulated damage in the as-implanted and annealed crystals. In particular, the disorder at the maximum of the damage peak (which is still located at ~130 nm) measured after annealing (~0.6) is twice that measured for the as-implanted crystal.

Fig. 2 displays the XRD curve recorded on the annealed crystal. Two major modifications, as compared to the as-implanted data, are observed: (i) a shift of the signal diffracted by the implanted layer towards the Bragg peak of the bulk undamaged YSZ and (ii) the disappearance of the fringe pattern. These results indicate a strong, but not total, release of the normal elastic strain and a modification of the strain depth profile. The analysis of the rocking curves presented in the inset of Fig. 2 reveals a strong increase of the diffuse scattering after annealing. This result suggests an increase of the defect density and/or the formation of larger defects than those observed in the as-implanted crystal. This latter statement is more consistent with the increase of the disorder level evidenced by RBS/C.

Fig. 3b presents an XTEM micrograph recorded on the annealed crystal. The damaged layer exhibits a highly defective zone located around the mean He-ion projected range (between ~100 and ~170 nm). This region contains both He bubbles and elongated fractures. The presence of this highly defective zone is consistent with the large increase of f_D at this depth (see Fig. 1b). This micrograph was taken using off-Bragg and underfocus imaging conditions which allow evidencing Fresnel fringes around bubbles (but lead to the suppression of strain field contrasts). Nevertheless, such contrasts were observed in two-beam conditions, meaning that strain fields are still present despite the formation of fractures.

4. Discussion

Results obtained with the three complementary techniques used in this work show that implantation of a high He concentration (~4 at.%) in YSZ induces only a weak damage of the crystalline

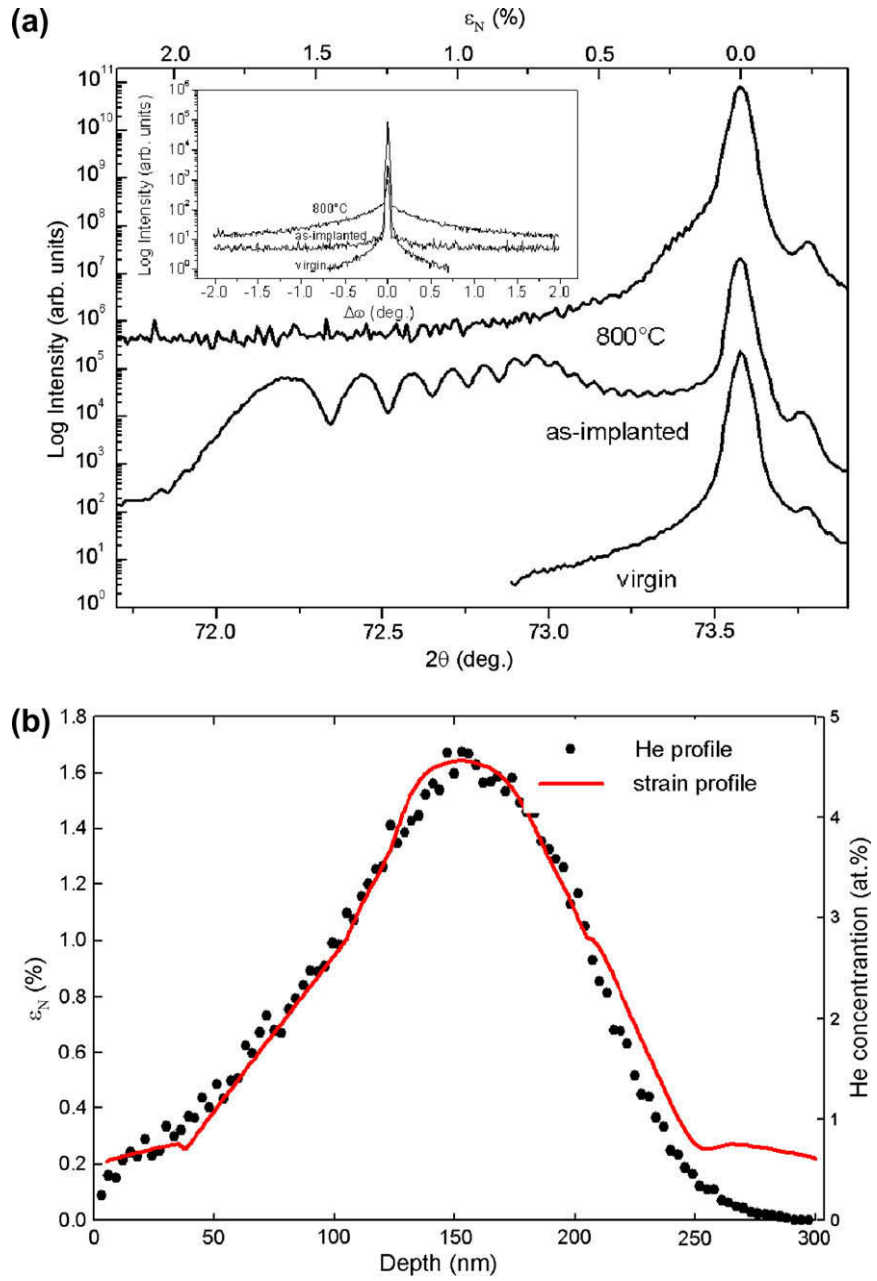

Fig. 2. (a) X-ray scattered intensity distribution in the vicinity of the (4 0 0) Bragg reflection on YSZ single crystals implanted at RT with 30 keV He ions at 5×10^{16} cm^{-2} and annealed for 1 h at 800 °C. The XRD curve of a virgin crystal is also displayed. (b) Experimental strain depth profile obtained from (a) and SRIM-predicted He depth distribution in YSZ implanted with 30 keV He ions at 5×10^{16} cm^{-2}.

structure, which is consistent with previous studies [6–13]. Actually, the disorder level measured by RBS/C in this work ($f_D \sim 0.3$) corresponds to the beginning of the second step of the damage build-up [6–13], where the He concentration is the key parameter for the matrix destabilization. This damage induces the development of a positive elastic strain, as measured by XRD. The defects at the origin of this strain must have a positive relaxation volume [23,24]. Two types of defects can be invoked in the current case: (i) He-vacancy complexes and (ii) self-interstitial atoms (SIAs), either directly created by ballistic collisions during the (nuclear) slowing-down of He ions, or indirectly formed during the growth of He-vacancy clusters that can push regular lattice atoms out of their equilibrium position. Since the depth strain profile overlaps the He depth distribution, it appears very likely that the defects directly related to the presence of He atoms play a major role on the crystalline distortions.

Upon annealing at 800 °C, a significant increase of the disorder level is observed by RBS/C. This result means that the energy brought during the thermal treatment did not induce defect recovery but on the contrary led to drastic microstructural modifications. Generally, in the case of ion implantation in YSZ (with e.g. Yb [25], Pt [26] or Cs [27,28]), post-implantation annealing leads to damage recovery (starting from 400 °C to 800 °C for Pt or Cs implantation, respectively). But in the particular case of inert gases, and especially He, the situation is different, since an increase of the disorder level is measured. Such a result was also observed (using positron annihilation spectroscopy) by Damen et al. [8,9] for 30 keV He implantation at concentrations larger than 1 at.%. The

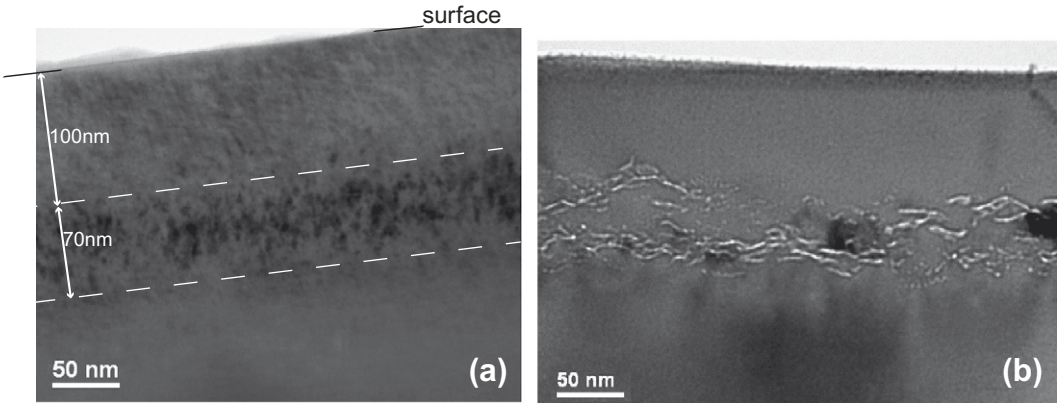

Fig. 3. TEM micrographs recorded on: (a) a YSZ single crystal implanted at RT with 30 keV He ions at 5×10^{16} cm^{-2} and (b) subsequently annealed for 1 h at 800 °C.

authors attributed this result to the growth of the small He-vacancy clusters produced during implantation which led to the formation of He bubbles. The same interpretation was also proposed in other studies to account for similar results (see e.g. [10]). However, no images of He bubbles were shown. As evidenced in Fig. 3b, in the current work TEM does reveal the presence of He bubbles after annealing. Therefore, the scenario proposed in previous studies is clearly verified, and it also holds in our case. It is worth noticing that the implanted layer is found to be highly damaged up to the surface (see RBS/C results of Fig. 1b), contrarily to what was observed just after implantation. The presence of small He-vacancy complexes up to the surface, not detectable by TEM, may explain this result. ERDA measurements are currently in progress to determine the He depth distributions. TEM also revealed the formation of fractures (see Fig. 3b) located at the maximum of the damage distribution. It is likely that these fractures developed to relax the stress generated by the presence of large over-pressurized He bubbles. The presence of extended defects, such as He bubbles and fractures, implies huge crystalline distortions which may explain both the large increase of the diffuse X-ray scattering and the elastic strain release. The strain relaxation may also arise from SIAs recombination or annihilation at defect sinks. However, it is interesting to note that the strain relaxation is not fully achieved after annealing at 800 °C, despite the formation of large cracks. This result is consistent with the presence of strain fields revealed by TEM. It suggests that further deleterious microstructural modifications should occur when increasing the annealing temperature.

5. Conclusion

The study of the microstructural modifications induced in yttria-stabilized zirconia single crystals implanted with low-energy (30 keV) He ions at a high He concentration (~4 at.%) has been addressed. In particular, the effect of post-implantation thermal annealing (at 800 °C) on the matrix integrity has been investigated. After implantation, the maximum accumulated damage fraction determined by RBS/C is small (~0.3). The damage very likely consists of interstitial-type defects with a small dimension and of helium-vacancy clusters. These defects induce a tensile elastic strain gradient with a maximum strain of ~1.6%. The shape of the strain depth profile corresponds to that of the SRIM-predicted He depth distribution. Post-implantation thermal annealing at 800 °C induces a partial strain relaxation but leads to a more damaged structure. Helium bubbles and elongated fractures, essentially located at a depth corresponding to the He projected range, are observed by TEM.

Finally, these experiments show that the crystalline structure of the zirconia matrix is resistant to the introduction of a rather high concentration of He atoms (~4 at.%) with a quite severe damage dose (~1.7 dpa). Nevertheless, submitted to a temperature increase (800 °C), the matrix exhibits a strong loss of integrity which could lead to a release of the incorporated radionuclides. These results should thus be taken into account for the design and use of this material as a storage matrix for nuclear waste.

Acknowledgments

We would like to warmly thank S. Moll for her help during TEM sample preparation, as well as the JANNuS-Orsay staff for assistance during ion implantation and RBS/C experiments. This work was partially supported by the GDR NOMADE, the scientific collaboration between IN2P3 and Romanian Laboratories, and also by the Romanian Ministry of Education and Research under PN II Program Grant No. 71-103.

References

[1] Hj. Matzke, Nucl. Instrum. Meth. B 116 (1996) 121.
[2] W.J. Weber, R.C. Ewing, C.R.A. Catlow, T. Diaz de la Rubia, L.W. Hobbs, C. Kinoshita, Hj. Matzke, A.T. Motta, M. Nastasi, E.K.H. Salje, E.R. Vance, S.J. Zinkle, J. Mater. Res. 13 (1998) 1434.
[3] C. Degueldre, J.M. Paratte, Nucl. Technol. 123 (1998) 21.
[4] K.E. Sickafus, Hj. Matzke, Th. Hartmann, K. Yasuda, J.A. Valdez, P. Chodak III, M. Nastasi, R.A. Verall, J. Nucl. Mater. 274 (1999) 66.
[5] W.L. Gong, W. Lutze, R.C. Ewing, J. Nucl. Mater. 277 (2000) 239.
[6] L. Thomé, J. Fradin, J. Jagielski, A. Gentils, S.E. Enescu, F. Garrido, Eur. Phys. J.: Appl. Phys. 24 (2003) 37.
[7] H. Trinkaus, B.N. Singh, J. Nucl. Mater. 323 (2003) 229–242.
[8] P.M.G. Damen, Hj. Matzke, C. Ronchi, J.-P. Hiernaut, T. Wiss, R. Fromknecht, A. Van Veen, F. Labohm, Nucl. Instrum. Meth. B 191 (2002) 571.
[9] P.M.G. Damen, A. van Veen, F. Labohm, H. Schut, M.A. van Huis, J. Nucl. Mater. 319 (2003) 65.
[10] S. Saudé, R.I. Grynszpan, W. Anwand, G. Brauer, J.J. Grob, Y. Le Gall, Nucl. Instrum. Meth. B 216 (2004) 156.
[11] J.M. Costantini, J.-J. Grob, J. Haussy, P. Trocellier, Ph. Trouslard, J. Nucl. Mater. 321 (2003) 281.
[12] R.I. Grynszpan, G. Brauer, W. Anwand, L. Malaquin, S. Saudé, I. Vickridge, E. Briand, Nucl. Instrum. Meth. B 261 (2007) 888.
[13] F. Garrido, L. Vincent, L. Nowicki, G. Sattonnay, L. Thomé, Nucl. Instrum. Meth. B 266 (2008) 2842.
[14] N. Sasajima, T. Matsui, S. Furuno, T. Shiratori, K. Hojou, Nucl. Instrum. Meth. B 166 (2000) 250.
[15] G. Kuri, M. Döbeli, D. Gavillet, G. Kuri, M. Döbeli, D. Gavillet, Nucl. Instrum. Meth. B245 (2006) 445.
[16] J.F. Ziegler, J.P. Biersack, U. Littmark, The Stopping and Range of Ions in Solids, Pergamon, New York, 1985, <http://www.srim.org>.
[17] L. Nowicki, A. Turos, R. Ratajczak, A. Stonert, F. Garrido, Nucl. Instrum. Meth. B 240 (2005) 277.
[18] R. Anderson, S. Klepeis, J. Benedict, W.G. Vandygrift, M. Orndorff, in: A.G. Cullis, J.L. Hutchinson (Eds.), Microscopy of Semiconducting Materials, Proceedings of the Royal Microscopical Society Conference, IOP Publishing LTD, Bristol, 1989, p. 491.
[19] S. Moll, L. Thomé, G. Sattonnay, A. Debelle, L. Vincent, F. Garrido, J. Jagielski, J. Appl. Phys. 106 (2009) 073509.

[20] A. Debelle, A. Declémy, L. Vincent, F. Garrido, L. Thomé, J. Nucl. Mater. 396 (2010) 240.
[21] N. Sousbie, L. Capello, J. Eymery, Ch. Lagahe, F. Rieutord, J. Appl. Phys. 99 (2006) 103509.
[22] S. Leclerc, M.F. Beaufort, A. Declémy, J.F. Barbot, Appl. Phys. Lett. 93 (2008) 122101.
[23] The relaxation volume is the volume change of the crystal due to the distortion field of one defect.
[24] P. Ehrhart, K.H. Robrock, H.R. Schober, R.A. Johnson, A.N. Orlov, Physics of Radiation Effects in Crystals, Elsevier, 1986.
[25] M. Berti, A.V. Drigo, C. Cohen, J. Siejka, M.M. Tosic, Nucl. Instrum. Meth. 199 (1982) 605.
[26] D.X. Cao, D.K. Sood, I.G. Brown, Nucl. Instrum. Meth. B 91 (1994) 280.
[27] L. Thomé, A. Gentils, J. Jagielski, F. Garrido, T. Thomé, Vacuum 81 (2007) 1264.
[28] L. Vincent, L. Thomé, F. Garrido, O. Kaitasov, J. Nucl. Mater. 385 (2009) 431.